Separable zero energy topological edge states and nonzero energy gap states in the nonreciprocal Su-Schrieffer-Heeger model

Wen-Jie Geng,[1] Ya-Jun Wang,[1] Zhi-Xu Zhang,[2] Ji Cao,[1,*] Wen-Xue Cui,[1,3,†] and Hong-Fu Wang[1,‡]

[1]*Department of Physics, College of Science, Yanbian University, Yanji, Jilin 133002, People's Republic of China*

[2]*School of Physics, Harbin Institute of Technology, Harbin 150001, People's Republic of China*

[3]*State Key Laboratory of Surface Physics and Department of Physics, Fudan University, Shanghai 200433, People's Republic of China*

(Received 10 May 2023; revised 6 October 2023; accepted 6 October 2023; published 19 October 2023)

Complex energy eigenvalues and the non-Hermitian skin effect are two notable properties of non-Hermitian systems. These properties result in the localization of all eigenstates at the system boundaries, which can undermine the dynamic stability and experimental detection of topological edge states. In this paper, we investigate the one-dimensional non-Hermitian Su-Schrieffer-Heeger model with next-nearest-neighbor nonreciprocal hopping. By examining the energy spectrum and state distributions of the system, we demonstrate that the zero energy topological edge state and nonzero energy gap state can be distinguished from the non-Hermitian skin states. Additionally, we analyze the localization properties of these two states using the directional inverse participation ratio and investigate the non-Hermitian skin effect through the energy spectrum on the complex plane and the spectral winding number. Furthermore, we present phase diagrams of separation factor that illustrate the separation phenomenon between the edge or gap state and skin states. This work reveals the intriguing relationship between topological properties and non-Hermitian skin effects in one-dimensional nonreciprocal systems.

DOI: 10.1103/PhysRevB.108.144109

I. INTRODUCTION

Condensed matter physics is a field that has emerged from solid-state physics and has gained significant importance in modern physics. As early as 1980, Von Klitzing discovered the quantum integer Hall effect in the two-dimensional electron gas system, which is a typical topological phase of matter in the two-dimensional electron gas system [1–4]. Subsequently, the concept of the Berry phase leads to the vigorous development of the study of the topological phase and topological phase transition [5,6]. The discovery of topological insulators has garnered extensive attention and has become a new research field in condensed matter physics [7–11]. Topological insulators exhibit unique physical properties, including nonconductive bulk states and a conductive zero mode on their surface. These conductive edge states are protected by the energy gap and are robust to local impurities, disorders, or perturbations [12–18]. Topological insulators possess unique topological invariants, such as winding number [19,20], Zak phase [21,22], and Chern number [23,24], which characterize their topological properties. These materials exhibit unidirectional transmission and back scattering suppression of electrons on their surface, making them ideal for applications in quantum information processing [25–27].

Recently, non-Hermitian systems have had a more comprehensive range of applications in efficiently describing classical or quantum open systems than Hermitian systems [28,29]. In constructing non-Hermitian systems, gain-loss, and nonreciprocal coupling methods are typically used. Recently, the study of non-Hermitian topological systems has further advanced the understanding of topological insulators [30,31]. However, introducing non-Hermitian terms can break the traditional bulk-boundary correspondence, which makes all of the eigenstates of the system localized at the boundary in the form of exponential decay [32]. Nevertheless, this issue can be overcome by creating a generalized Brillouin zone, thus restoring the bulk-boundary correspondence [33]. Furthermore, many kinds of research focused on using a new method for describing the topological properties of the non-Hermitian skin effect (NHSE) and the design of multidirectional transport topological devices [34–36]. On the other hand, the Su-Schrieffer-Heeger (SSH) model is a widely studied one-dimensional (1D) lattice system that describes the hopping of electrons in a chainlike structure [37]. Initially used to describe polyacetylene, this model is simple in structure and has rich topological properties. Hence, the non-Hermitian extension of the SSH model has again become a research hot area in theory and experiment [38–40]. For example, introducing balanced gain and loss creates a non-Hermitian system that satisfies the parity-time symmetry [41–46] or asymmetric coupling to create a nonreciprocal hopping [47–51]. Moreover, the SSH model has been simulated in many physical systems, such as electronic circuit systems [52], acoustic systems [53], optical superlattice [54], atomic systems [55], and quantum dot arrays [56].

In the non-Hermitian topological system, the experimental detection of topological edge states with complex energies

*caoji@ybu.edu.cn

†cuiwenxue@ybu.edu.cn

‡hfwang@ybu.edu.cn

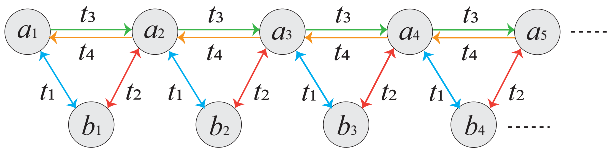

FIG. 1. Diagrammatic sketch of the 1D non-Hermitian SSH model with next-nearest-neighbor nonreciprocal hopping. Each unit cell has two sites, labeled as a_j and b_j, respectively. Blue and red arrows denote the nearest-neighbor hopping strengths t_1 and t_2. Yellow and green arrows represent the next-nearest-neighbor nonreciprocal hopping strengths with $t_3 = t + \delta\cos\theta$ and $t_4 = t - \delta\cos\theta$, respectively.

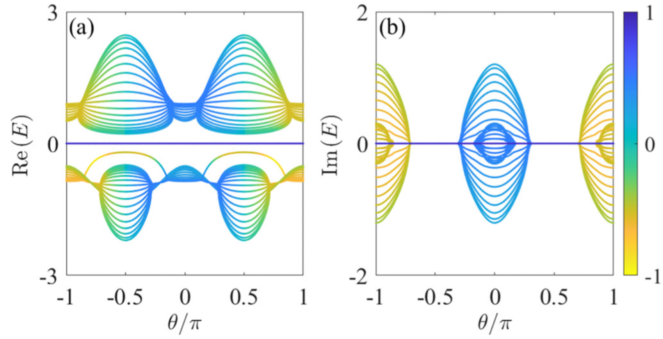

FIG. 2. Energy spectrum of the system as a function of θ under OBC. The parameters are set as $t_1 = 0.2$, $t_2 = 0.9$, $\delta = 1.3$, $\eta = -1$, and $L = 40$, respectively.

is challenging due to dynamic instability. Another challenge is distinguishing between topological edge states and bulk states, as NHSE causes all bulk states localized at the boundaries with exponential decay. In this paper, we study the 1D non-Hermitian SSH model with next-nearest-neighbor nonreciprocal hopping. Through analysis of the energy spectrum and state distributions, the zero energy topological edge state and nonzero energy gap state can be distinguished from the non-Hermitian skin states. The localization properties of the zero energy topological edge state and nonzero energy gap state under OBC are investigated using the directional inverse participation ratio (dIPR). Additionally, the localization behavior of the non-Hermitian skin states is connected to the surrounding directions of the spectrum on the complex energy plane under periodic boundary conditions (PBC). Furthermore, a phase diagram of separation factor is shown to visually illustrate the separation phenomenon between the edge or gap state and the skin states.

The paper is organized as follows. In Sec. II, we give the model and Hamiltonian of the system. In Sec. III, we investigate the energy spectrum and state distributions of the 1D non-Hermitian SSH model with next-nearest-neighboring hopping. In Sec. IV, we analyze and demonstrate the separation phenomenon between the zero energy topological edge state, nonzero energy gap state, and non-Hermitian skin states by using phase diagrams with separation factor. Finally, a conclusion is given in Sec. V.

II. MODEL AND HAMILTONIAN

We consider a 1D non-Hermitian SSH model with next-nearest-neighbor nonreciprocal hopping, as illustrated in Fig. 1. The total Hamiltonian of the system can be described as follows:

$$H^{(\eta)} = H_0 + H_1^{(\eta)}, \tag{1}$$

with

$$\begin{aligned} H_0 = \sum_{j=1}^{N} [& t_1(a_j^\dagger b_j + b_j^\dagger a_j) + t_2(b_j^\dagger a_{j+1} + a_{j+1}^\dagger b_j) \\ & + t_3 a_{j+1}^\dagger a_j + t_4 a_j^\dagger a_{j+1}], \end{aligned} \tag{2}$$

$$H_1^{(\eta)} = \eta[t_2(a_{N+1}^\dagger b_N + b_N^\dagger a_{N+1}) + t_3 a_{N+1}^\dagger a_N + t_4 a_N^\dagger a_{N+1}], \tag{3}$$

where $a_j^\dagger(a_j)$ and $b_j^\dagger(b_j)$ represent the creation (annihilation) operators of the jth site of the system. For $\eta = -1$, it means the even-sized system $L = 2N$, and $\eta = 0$ indicates the odd-sized system $L = 2N + 1$, in which N is the number of unit cells. t_1 and t_2 are the nearest-neighbor hopping strengths. $t_3 = t + \delta\cos\theta$ and $t_4 = t - \delta\cos\theta$ are the next-nearest-neighbor nonreciprocal hopping, where $\theta \in [0, 2\pi]$ is the periodic parameter and δ is the nonreciprocal amplitude. When the nonreciprocal hopping terms in Eq. (1) are equal to 0 ($t_3 = t_4 = 0$), the current system can be identified as a standard SSH model. As a result of the odd-sized lattice sites, the system exhibits zero energy topological edge states throughout the whole parameter space. For even-sized lattice sites, two degenerate zero energy topological edge states localized at the end of the system. Here, we aim at the situation for $t_3 \neq t_4$. For simplicity, we choose $t = 1$ as the energy unit in all of the paper.

III. ENERGY SPECTRUM AND STATE DISTRIBUTIONS

In this section, we first explore the energy spectrum and state distributions of the 1D non-Hermitian SSH model with next-nearest-neighbor nonreciprocal hopping. The current system exhibits the NHSE due to the introduction of next-nearest-neighbor nonreciprocal hopping. As shown in Fig. 2, we demonstrate the energy spectrum of the even-sized SSH model as a function of θ under open boundary conditions (OBC) with $t_1 = 0.2$, $t_2 = 0.9$, $\delta = 1.3$, and $L = 40$, respectively. It is found that the current system holds one zero energy topological edge state throughout the whole parameter regions θ. Additionally, one nonzero energy gap state exists in the system within $0.16\pi < |\theta| < 0.84\pi$. To characterize the localization properties of all eigenstates, we introduce the dIPR featuring the energy spectrum as [51]

$$\text{dIPR}(\psi_\text{n}) = \mathcal{P}(\psi_n)\frac{\sum_{j=1}^{L}|\psi_{n,j}|^4}{\left(\sum_{j=1}^{L}|\psi_{n,j}|^2\right)^2}, \tag{4}$$

with $\mathcal{P}(\psi_n)$ defined as

$$\mathcal{P}(\psi_n) = \text{sgn}\left[\sum_{j=1}^{L}\left(j - \frac{L}{2} - \alpha\right)|\psi_{n,j}|\right], \tag{5}$$

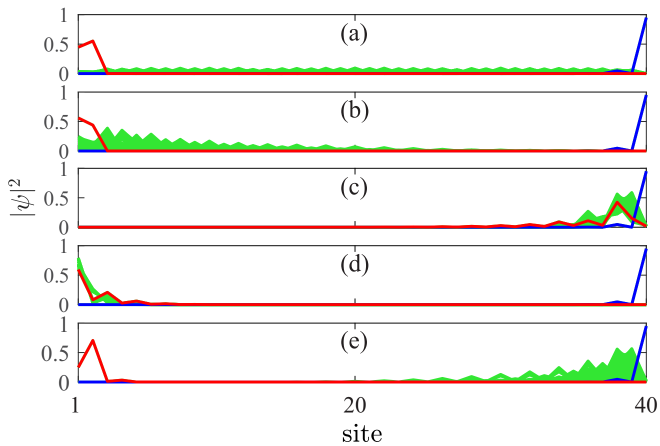

FIG. 3. State distributions of the system with $t_1 = 0.2$, $t_2 = 0.9$, $\delta = 1.3$, $L = 40$, and $\eta = -1$. Other parameters are taken as (a) $\theta = 0.5\pi$, (b) $\theta = 0.55\pi$, (c) $\theta = 0.18\pi$, (d) $\theta = \pi$, and (e) $\theta = 0.37\pi$. The red, green, and blue lines present the nonzero energy gap state, the bulk state, and the zero energy topological edge state distributions, respectively.

where $|\psi_n\rangle_j$ is the jth eigenstate of the system with energy eigenvalue E_n. α is a constant value, which is normally determined as $0 < \alpha < 0.5$. sgn(x) denotes the sign function, making sgn(x) = 1 for $x > 0$ and sgn(x) = 1 for $x < 0$. The value of dIPR is positive or negative corresponding to the right or left localization, respectively. One can see that the values of dIPR for bulk states are positive within $|\theta| < 0.5\pi$, indicating the right localization of the eigenstates; the negative case for $|\theta| > 0.5\pi$, indicating the left localization of the eigenstates. When $|\theta| = 0.5\pi$, the dIPR of the bulk states is close to 0, representing that the bulk states converge toward extended states. However, the value of dIPR for the zero energy topological edge state is close to 1 throughout the whole parameter region θ, corresponding to the highly localized at the right boundary of the system. We further reveal that the nonzero energy gap states will be shifted from right localization to left localization as $|\theta|$ increases with the critical value $|\theta| = 0.207\pi$.

Furthermore, we present the state distributions of the system in Fig. 3. We find that the zero energy topological edge state, nonzero energy gap state, and bulk states coexist. For $\theta = 0.5\pi$, the current system reduces to a Hermitian SSH model with next-nearest-neighbor hopping. It is found that the nonzero energy gap state and the zero energy topological edge state are localized at opposite boundaries of the system and the bulk states are extended, as shown in Fig. 3(a). Then, for $\theta = 0.55\pi$, the current system is a non-Hermitian system with next-nearest-neighbor nonreciprocal hopping. From Fig. 3(b), it is found that the gap state and edge state are also localized at opposite boundaries of the system. However, for $\theta = 0.18\pi$, all the eigenstates are right localization, the same as general NHSE with all the states localized at one boundary in Fig. 3(c). Interestingly, for the non-Hermitian case with $\theta = \pi$, we can reveal the separation of the zero energy topological edge state from skin states and the nonzero energy gap state, highly localizing at the end of the lattice, as shown in Fig. 3(d). One can see that the zero energy topological edge state is localized at the right boundary of the system, and the skin states are localized at the left boundary of the system. The topological edge state with zero energy ensures dynamic stability and experimental detection. Moreover, for $\theta = 0.37\pi$, the nonzero energy gap state can be separated from skin states and the zero energy topological edge state, localizing with opposite directions in Fig. 3(e). One can see that the nonzero energy gap state is left localization, and the skin states are right localization.

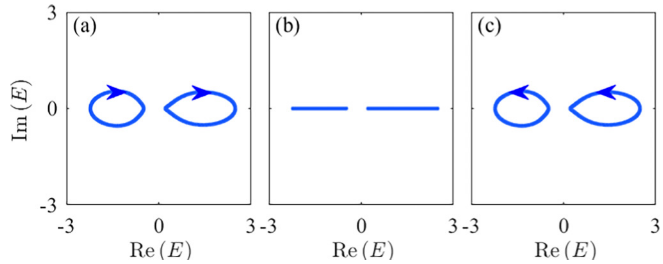

FIG. 4. Energy spectrum on the complex plane under PBC with $t_1 = 0.2$, $t_2 = 0.9$, $\delta = 1.3$, $L = 40$, $N = 20$, and $\eta = -1$. The other parameters are set as (a) $\theta = 0.4\pi$, (b) $\theta = 0.5\pi$, and (c) $\theta = 0.6\pi$, respectively. The arrow represents the surrounding direction of the energy spectrum on the complex plane.

IV. CHARACTERIZATION OF SEPARABLE ZERO ENERGY TOPOLOGICAL EDGE STATES AND NONZERO ENERGY GAP STATES

In this section, we investigate non-Hermitian skin phase transition of system and its characterization in the even-sized SSH model under PBC. In momentum space, the Bloch Hamiltonian of the system can be written as $H = \sum_k \psi(k)^\dagger H(k)\psi(k)$ with $\psi(k) = (a_k, b_k)^T$, and $H(k)$ is

$$H(k) = h_0 I + h_x\sigma_x + h_y\sigma_y + h_0\sigma_z, \tag{6}$$

where $h_0 = \cos k - i\delta\cos\theta\sin k$, $h_x = t_1 + t_2\cos k$, and $h_y = t_2\sin k$. The energy eigenvalue of the system can be obtained by

$$E_\pm(k) = h_0 \pm \sqrt{h_0^2 + h_x^2 + h_y^2}. \tag{7}$$

For $k = 0$ or $k = \pi$, there are four points with pure real energies, which are independent of the value of θ. In the following, we calculate the four fixed points and determine the range of the energy reference point to calculate the winding number.

We first focus on the energy spectrum on the complex plane of the system with $t_1 = 0.2$, $t_2 = 0.9$, $\delta = 1.3$, and $L = 40$, as shown in Fig. 4. The energy eigenvalues of the system have been obtained by Eq. (7). For an invertible non-Hermitian $H(k)$, if and only if the real or imaginary part of all the eigenenergies is nonzero, $H(k)$ is defined to have a line gap (real or imaginary band gap) in the real or imaginary part of its complex spectrum [57]. When $\theta = 0.4\pi$, there are two loops with clockwise rotation on the complex energy plane holding a line gap in Fig. 4(a), corresponding to all the bulk states localized at the right boundary of the system shown in Fig. 4(a). For $\theta = 0.5\pi$, the nonreciprocal terms become $t_3 = t_4$, resulting in the Hamiltonian of the system becoming Hermitian. Correspondingly, two line-gapped bands exist on the real axis of the complex energy plane. When θ is up

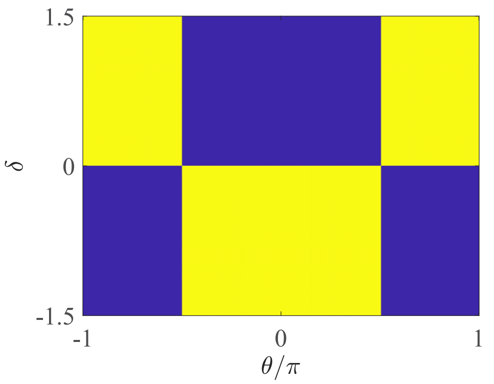

FIG. 5. Phase diagram of the spectral winding number for phase transition of the non-Hermitian skin effect of the system with $t_1 = 0.2$, $t_2 = 0.9$, $N = 20$, $\eta = -1$, and $L = 40$. The spectral winding numbers $W = -1$ with blue areas and $W = 1$ with yellow areas represent right and left localization of NHSE, respectively.

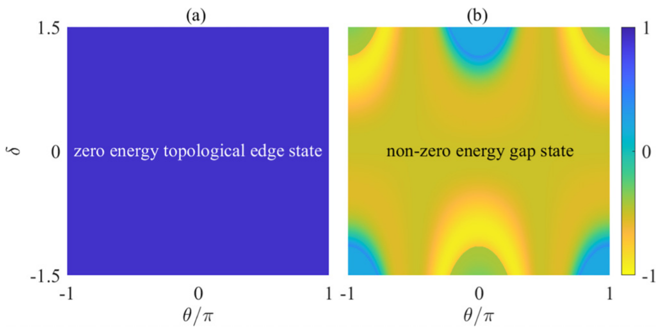

FIG. 6. Localization phase diagram of (a) zero energy edge state and (b) nonzero energy gap state, respectively. The color bar indicates the dIPR of the eigenstates. The parameters chosen are the same as Fig. 5.

to 0.6π, it can be observed that the eigenenergies form two loops on the complex energy plane, and the energy spectrum holds a line gap, as shown in Fig. 4(c). However, different from Fig. 4(a), the corresponding complex spectrum profiles are surrounded with counter-clockwise rotation, and all the bulk states are localized at the left boundary of the system. Hence, the eigenenergies of the system undergo a complex-real-complex phase transition accompanied by the closing and reopening of band gaps on the complex energy plane. Furthermore, it is found that the skin effect exhibits phase transition with the bulk states shifted from right localization to left localization accompanied by the clockwise rotation shifted to counterclockwise rotation of the energy spectrum.

In order to present an accurate description of the above phase transition of NHSE, we adopt a method to establish the connection between the spectral winding number and the localization of bulk states. The spectral winding number is defined as [58,59]

$$W = \int_{-\pi}^{\pi} \frac{\mathrm{d}k}{2\pi i} \partial k \ln \det[H(k) - E_0], \tag{8}$$

where E_0 is the energy reference point. The winding number under PBC can accurately predict the localization directions of bulk states under OBC. The case of $W = -1$ and $W = 1$ represent that the energy reference point is surrounded in clockwise and counter-clockwise directions on the complex energy plane, respectively. The energy reference point is not surrounded, indicating no loop structure in the spectrum, resulting in $W = 0$. Then, we choose the appropriate range of energy reference points. By calculating Eq. (5), four pure real energies exist on the complex energy plane, with

$$E_\pm(0) = 1 \pm \sqrt{1 + (t_1 + t_2)^2},$$
$$E_\pm(\pi) = -1 \pm \sqrt{1 + (t_1 - t_2)^2}, \tag{9}$$

where the values of the energy reference points are in the range of $E_0 \in [E_+(\pi), E_+(0)] \cup [E_-(\pi), E_-(0)]$. As shown in Fig. 5, we plot the phase diagram for the spectral winding number of the system versus θ with $t_1 = 0.2$, $t_2 = 0.9$, $\delta = 1.3$, and $L = 40$. For $E_0 \in (-1 + \sqrt{1.49}, 1 + \sqrt{2.21})$ or $E_0 \in (-1 - \sqrt{1.49}, 1 - \sqrt{2.21})$, and the winding number can correctly predict the localized directions of the bulk states. For the regions of $0.5\pi < |\theta| < \pi$ within $\delta > 0$, and $|\theta| < 0.5\pi$ within $\delta < 0$, the winding number $W = 1$ for the yellow regions of the phase diagram corresponds to the energy reference point surrounded by the complex spectrum profile in a counter-clockwise direction. It represents that the bulk states are localized at the left boundary of the system. When $|\theta| < 0.5\pi$ within $\delta > 0$, and $0.5\pi < |\theta| < \pi$ within $\delta < 0$, the right localization of bulk states corresponds to the energy reference point, which is surrounded by the complex spectrum profile in a clockwise direction, resulting the winding number $W = -1$ for the blue regions in the phase diagram. For $\theta = \pm 0.5\pi$, the energy reference point is not surrounded by the complex spectrum profiles, indicating $W = 0$. The above results indicate that $W = 1$ and $W = -1$ represent the left and right localization of bulk states, respectively. Moreover, the system undergoes skin phase transition with $\theta = \pm 0.5\pi$ and $\delta = 0$, which together constitute the phase transition boundary of the system.

Next, we turn to the localization phase of zero energy topological edge state and nonzero energy gap state, as shown in Fig. 6. It is found that the dIPR of the zero energy edge state is constantly close to 1 in Fig. 6(a). This phenomenon indicates that the zero energy topological edge state is highly localized at the right end of the lattice through the whole parameters regions, which differs from the case of bulk states possessing both right localization and left localization, as shown in Fig. 5. The different localization behavior of the zero energy topological edge state and bulk states implies that the zero energy topological edge state can be separated from the bulk states in certain parameter regions. On the other hand, we demonstrate the localization phase of the nonzero energy gap state in Fig. 6(b). The blue and yellow regions correspond to the right and left localization of the nonzero energy gap state in Fig. 6(b), respectively. It is found that the system holds the right localized nonzero energy gap state within $1.04 < |\delta| < 1.5$. Compared with Fig. 5, one can see that the phase boundary for the nonzero energy gap state is different from that for the bulk states, which implies the system holds a separable nonzero energy gap state for specific parameter conditions. The transition of the localization phase

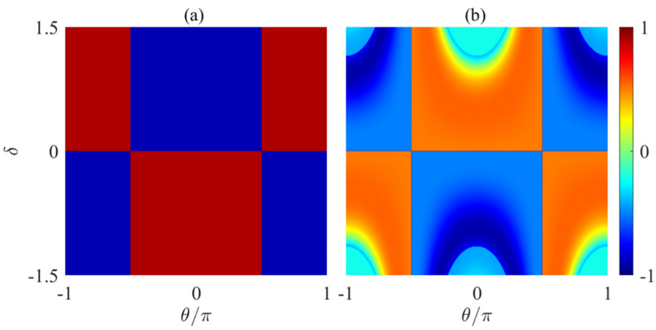

FIG. 7. Phase diagram of separation factor $S(\psi_n)$ for (a) zero energy topological edge state and (b) nonzero energy gap state, respectively. The color bar indicates the value of separation factor for the eigenstates. The parameters chosen are the same as Fig. 5.

for the nonzero energy gap state is due to the introduction of the next-nearest-neighbor nonreciprocal hopping.

To further characterize the separable zero energy topological edge state and nonzero energy gap state, we define the separation factor as $S(\psi_n) = W \cdot \mathrm{dIPR}(\psi_\mathrm{n})$, whose essence originates from the localized direction information of eigenstates of the system. ψ_n represents the zero energy topological edge state or nonzero energy gap state. As mentioned above, $W = -1$ ($W = 1$) represents the right (left) localization of bulk states, and the value of dIPR is positive (negative) for the eigenstate exhibiting right (left) localization. For $S(\psi_n) > 0$, the zero energy topological edge state and nonzero energy gap state are separated from the bulk states. Otherwise, these two states and bulk states are both localized at one boundary of the system for $S(\psi_n) < 0$. As shown in Fig. 7(a), we demonstrate the separable phase for the zero energy topological edge state. For the red regions of $0.5\pi < |\theta| < \pi$ within $\delta > 0$, and $|\theta| < 0.5\pi$ within $\delta < 0$, $S(\psi_n)$ is close to 1, corresponding to the right localization phase of the zero energy topological edge state. It is indicated that the zero energy topological edge state is always localized at the opposite boundary of the system, which is consistent with the results of our previous analysis in Figs. 3(b) and 3(d). For $|\theta| < 0.5\pi$ within $\delta > 0$, and $0.5\pi < |\theta| < \pi$ within $\delta < 0$, the blue regions represent the zero energy topological edge state and bulk states are both localized at one boundary of the system, discussed in Figs. 3(c) and 3(e). As shown in Fig. 7(b), we show the phase diagram of separation factor $S(\psi_n)$ for the nonzero energy gap state of the system. We find that the orange and yellow regions correspond to the $S(\psi_n) > 0$, which represents the separated nonzero energy gap state shown in Fig. 3(e). The blue regions with $S(\psi_n) < 0$ represent the nonzero energy gap state, and bulk states are both localized at one boundary of the system, discussed Figs. 3(b)–3(d).

V. CONCLUSIONS

In conclusion, we have investigated the 1D non-Hermitian SSH model with next-nearest-neighbor nonreciprocal hopping. By examining the energy spectrum and state distributions, we found that the system holds a zero energy topological edge state and nonzero energy gap state in an even-sized system. We analyzed the localization properties of these two states using the directional inverse participation ratio. Under specific parameter conditions, these two states can be distinguished from the non-Hermitian skin states. We also studied the energy spectrum on the complex plane and utilized the spectral winding number to illustrate the phase transition of the NHSE of the system. We constructed a phase diagram of separation factor $S(\psi_n) = W \cdot \mathrm{dIPR}(\psi_\mathrm{n})$ to further reveal the separation phenomenon between the edge or gap state and the skin states. Our work further reveals the intriguing combination of topological properties and non-Hermitian skin effects in 1D nonreciprocal systems.

ACKNOWLEDGMENTS

This work was supported by the National Natural Science Foundation of China under Grants No. 62301472, No. 12375020, No. 12074330, and No. 62201493; the Natural Science Foundation of Jilin Province under Grant No. YDZJ202201ZYTS298; the Science and Technology Project of Education Department of Jilin Province under Grant No. JJKH20220530KJ; the Young Talents Support Project of Association of Science and Technology of Jilin Province under Grant No. QT2021029.

[1] K. V. Klitzing, G. Dorda, and M. Pepper, New method for high-accuracy determination of the fine-structure constant based on quantized Hall resistance, Phys. Rev. Lett. **45**, 494 (1980).
[2] Y. Hatsugai, Chern number and edge states in the integer quantum hall effect, Phys. Rev. Lett. **71**, 3697 (1993).
[3] D. J. Thouless, Edge voltages and distributed currents in the quantum hall effect, Phys. Rev. Lett. **71**, 1879 (1993).
[4] D. J. Thouless, Topological interpretations of quantum Hall conductance, J. Math. Phys. **35**, 5362 (1994).
[5] M. V. Berry, Quantal phase factors accompanying adiabatic changes, Proc. R. Soc. London A **392**, 45 (1984).
[6] A. Tomita and R. Y. Chiao, Observation of Berry's topological phase by use of an optical fiber, Phys. Rev. Lett. **57**, 937 (1986).
[7] X. L. Qi and S. C. Zhang, Topological insulators and superconductors, Rev. Mod. Phys. **83**, 1057 (2011).
[8] A. Bansil, H. Lin, and T. Das, Topological band theory, Rev. Mod. Phys. **88**, 021004 (2016).
[9] Z. Xu, Y. Zhang, and S. Chen, Topological phase transition and charge pumping in a one-dimensional periodically driven optical lattice, Phys. Rev. A **96**, 013606 (2017).
[10] L. Li, Z. Xu, and S. Chen, Topological phases of generalized Su-Schrieffer-Heeger models, Phys. Rev. B **89**, 085111 (2014).
[11] L. Li and S. Chen, Characterization of topological phase transitions via topological properties of transition points, Phys. Rev. B **92**, 085118 (2015).
[12] F. Mei, S. L. Zhu, Z. M. Zhang, C. H. Oh, and N. Goldman, Simulating Z_2 topological insulators with cold atoms in a

one-dimensional optical lattice, Phys. Rev. A **85**, 013638 (2012).

[13] Z. Xu, R. Zhang, S. Chen, L. Fu, and Y. Zhang, Fate of zero modes in a finite Su-Schrieffer-Heeger model with $\mathcal{PT}$ symmetry, Phys. Rev. A **101**, 013635 (2020).

[14] L. A. Wray, S. Y. Xu, Y. Xia, D. Hsieh, A. V. Fedorov, Y. S. Hor, R. J. Cava, A. Bansil, H. Lin, and M. Z. Hasan, A topological insulator surface under strong Coulomb, magnetic and disorder perturbations, Nat. Phys. **7**, 32 (2011).

[15] M. Malki and G. S. Uhrig, Tunable edge states and their robustness towards disorder, Phys. Rev. B **95**, 235118 (2017).

[16] E. Berg, E. G. D. Torre, T. Giamarchi, and E. Altman, Rise and fall of hidden string order of lattice bosons, Phys. Rev. B **77**, 245119 (2008).

[17] G. Y. Chitov, Local and nonlocal order parameters in the Kitaev chain, Phys. Rev. B **97**, 085131 (2018).

[18] C. E. Agrapidis, J. van. den. Brink, and S. Nishimoto, Ground state and low-energy excitations of the Kitaev-Heisenberg two-leg ladder, Phys. Rev. B **99**, 224418 (2019).

[19] L. Wang, X. Dai, and X. C. Xie, Frequency domain winding number and interaction effect on topological insulators, Phys. Rev. B **84**, 205116 (2011).

[20] J. Claes and T. L. Hughes, Skin effect and winding number in disordered non-Hermitian systems, Phys. Rev. B **103**, L140201 (2021).

[21] Q. Wang, M. Xiao, H. Liu, S. N. Zhu, and C. T. Chan, Measurement of the Zak phase of photonic bands through the interface states of a metasurface/photonic crystal, Phys. Rev. B **93**, 041415(R) (2016).

[22] X. X. Li, P. B. Li, H. R. Li, H. Gao, and F. L. Li, Simulation of topological Zak phase in spin-phononic crystal networks, Phys. Rev. Res. **3**, 013025 (2021).

[23] S. Yang, Z. C. Gu, K. Sun, and S. D. Sarma, Topological flat band models with arbitrary Chern numbers, Phys. Rev. B **86**, 241112(R) (2012).

[24] B. Huang, C. F. Chan, and M. Gong, Large Chern-number topological superfluids in a coupled-layer system, Phys. Rev. B **91**, 134512 (2015).

[25] Y. Xing, L. Qi, X. Zhao, Z. Lü, S. Liu, S. Zhang, and H. F. Wang, Quantum transport in a one-dimensional quasicrystal with mobility edges, Phys. Rev. A **105**, 032443 (2022).

[26] J. Seo, P. Roushan, H. Beidenkopf, Y. S. Hor, R. J. Cava, and A. Yazdani, Transmission of topological surface states through surface barriers, Nature (London) **466**, 343 (2010).

[27] C. Dlaska, B. Vermersch, and P. Zoller, Robust quantum state transfer via topologically protected edge channels in dipolar arrays, Quantum Sci. Technol. **2**, 015001 (2017).

[28] Z. X. Zhang, R. Huang, L. Qi, Y. Xing, Z. J. Zhang, and H. F. Wang, Topological phase transition and eigenstates localization in a generalized non-hermitian su-schrieffer-Heeger Model, Ann. Phys. **533**, 2000272 (2021).

[29] L. Qi, G. L. Wang, S. Liu, S. Zhang, and H. F. Wang, Robust interface-state laser in non-hermitian microresonator arrays, Phys. Rev. Appl. **13**, 064015 (2020).

[30] C. M. Bender and S. Boettcher, Real spectra in non-hermitian hamiltonians having $\mathcal{PT}$ symmetry, Phys. Rev. Lett. **80**, 5243 (1998).

[31] M. Ezawa, Braiding of Majorana-like corner states in electric circuits and its non-Hermitian generalization, Phys. Rev. B **100**, 045407 (2019).

[32] Y. Xiong, Why does bulk boundary correspondence fail in some non-Hermitian topological models, J. Phys. Commun. **2**, 035043 (2018).

[33] S. Yao and Z. Wang, Edge states and topological invariants of non-sermitian systems, Phys. Rev. Lett. **121**, 086803 (2018).

[34] S. Longhi, Topological phase transition in non-Hermitian quasicrystals, Phys. Rev. Lett. **122**, 237601 (2019).

[35] S. Longhi, Nonadiabatic robust excitation transfer assisted by an imaginary gauge field, Phys. Rev. A **95**, 062122 (2017).

[36] K. Xu, X. Zhang, K. Luo, R. Yu, D. Li, and H. Zhang, Coexistence of topological edge states and skin effects in the non-Hermitian Su-Schrieffer-Heeger model with long-range nonreciprocal hopping in topoelectric realizations, Phys. Rev. B **103**, 125411 (2021).

[37] W. P. Su, J. R. Schrieffer, and A. J. Heeger, Soliton in polyacetylene, Phys. Rev. Lett. **42**, 1698 (1979).

[38] W. G. Song, W. Z. Sun, C. Chen, Q. H. Song, S. M. Xiao, S. N. Zhu, and T. Li, Breakup and recovery of topological zero modes in finite non-hermitian optical lattices, Phys. Rev. Lett. **123**, 165701 (2019).

[39] Y. L. Song, Y. L. Chen, W. Xiong, and M. F. Wang, Flexible light manipulation in non-Hermitian frequency Su-Schrieffer-Heeger lattice, Opt. Lett. **47**, 1646 (2022).

[40] K. Liao, Y. G. Zhong, Z. C. Du, G. D. Liu, C. T. Li, X. X. Wu, C. H. Deng, C. C. Lu, X. Y Wang, C. T. Chan, Q. H. Song, S. F. Wang, X. F. Liu, X. Y. Hu, and Q. H. Gong, On-chip integrated exceptional surface microlaser, Sci. Adv. **9**, eadf3470 (2023).

[41] K. G. Makris, R. El-Ganainy, and D. N. Christodoulides, and Z. H. Musslimani, Beam Dynamics in $\mathcal{PT}$ Symmetric Optical Lattices, Phys. Rev. Lett. **100**, 103904 (2008).

[42] S. Longhi, Bloch oscillations in complex crystals with $\mathcal{PT}$ symmetry, Phys. Rev. Lett. **103**, 123601 (2009).

[43] Z. Lin, H. Ramezani, T. Eichelkraut, T. Kottos, H. Cao, and D. N. Christodoulides, Unidirectional invisibility induced by $\mathcal{PT}$-symmetric periodic structures, Phys. Rev. Lett. **106**, 213901 (2011).

[44] A. Guo, G. J. Salamo, D. Duchesne, R. Morandotti, M. Volatier-Ravat, V. Aimez, G. A. Siviloglou, and D. N. Christodoulides, Observation of $\mathcal{PT}$-symmetry breaking in complex optical potentials, Phys. Rev. Lett. **103**, 093902 (2009).

[45] J. B. Gong and Q. H. Wang, Geometric phase in $\mathcal{PT}$-symmetric quantum mechanics, Phys. Rev. A **82**, 012103 (2010).

[46] M. Klett, H. Cartarius, D. Dast, J. Main, and G. Wunner, Relation between $\mathcal{PT}$-symmetry breaking and topologically nontrivial phases in the Su-Schrieffer-Heeger and Kitaev models, Phys. Rev. A **95**, 053626 (2017).

[47] W. X. Cui, L. Qi, Y. Xing, S. T. Liu, S. Zhang, and H. F. Wang, Localized photonic states and dynamic process in nonreciprocal coupled Su-Schrieffer-Heeger chain, Opt. Express **28**, 37026 (2020).

[48] W. W. Zhu and J. B. Gong, Hybrid skin-topological modes without asymmetric couplings, Phys. Rev. B **106**, 035425 (2022).

[49] C. Sanavio, V. Peano, and A. Xuereb, Nonreciprocal topological phononics in optomechanical arrays, Phys. Rev. B **101**, 085108 (2020).

[50] Q. B. Zeng, Y. B. Yang, and R. Lü, Topological phases in one-dimensional nonreciprocal superlattices, Phys. Rev. B **101**, 125418 (2020).

[51] Q. B. Zeng and R. Lü, Real spectra and phase transition of skin effect in nonreciprocal systems, Phys. Rev. B **105**, 245407 (2022).

[52] S. Imhof, C. Berger, F. Bayer, J. Brehm, L. W. Molenkamp, T. Kiessling, F. Schindler, C. H. Lee, M. Greiter, T. Neupert, and R. Thomale, Topolectrical-circuit realization of topological corner modes, Nat. Phys. **14**, 925 (2018).

[53] Z. J. Yang, F. Gao, X. H. Shi, X. Lin, Z. Gao, Y. D. Chong, and B. L. Zhang, Topological acoustics, Phys. Rev. Lett. **114**, 114301 (2015).

[54] B. X. Wang and C. Y. Zhao, Topological photonic states in one-dimensional dimerized ultracold atomic chains, Phys. Rev. A **98**, 023808 (2018).

[55] M. Kiczynski, S. K. Gorman, H. Geng, M. B. Donnelly, Y. Chung, Y. He, J. G. Keizer, and M. Y. Simmons, Engineering topological states in atom-based semiconductor quantum dots, Nature (London) **606**, 694 (2022).

[56] N. Petropoulos, R. B. Staszewski, D. Leipold, and E. Blokhina, Topological order detection and qubit encoding in Su-Schrieffer-Heeger type quantum dot arrays, J. Appl. Phys. **131**, 074401 (2022).

[57] K. Kawabata, K. Shiozaki, M. Ueda, and M. Sato, Symmetry and topology in non-Hermitian physics, Phys. Rev. X **9**, 041015 (2019).

[58] Z. Lin, L. Ding, S. Ke, and X. Li, Steering non-Hermitian skin modes by synthetic gauge fields in optical ring resonators, Opt. Lett. **46**, 3512 (2021).

[59] K. Wang, A. Dutt, C. C. Wojcik, and S. Fan, Topological complex-energy braiding of non-Hermitian bands, Nature (London) **598**, 59 (2021).